THE JOURNAL OF PHYSICAL CHEMISTRY B

Article

pubs.acs.org/JPCB

Controlling Morphology and Chain Aggregation in Semiconducting Conjugated Polymers: The Role of Solvent on Optical Gain in MEH-PPV

Zach E. Lampert,*[,†] C. Lewis Reynolds, Jr.,[†] John M. Papanikolas,[‡] and M. Osama Aboelfotoh[†]

[†]Department of Materials Science and Engineering, North Carolina State University, Raleigh, North Carolina 27695-7919, United States

[‡]Department of Chemistry, University of North Carolina, Chapel Hill, North Carolina 27599, United States

ABSTRACT: We report the results of a detailed investigation that addresses the influence of polymer morphology and chain aggregation, as controlled by the chemical nature of the solvent, on the optical gain properties of the conjugated polymer poly[2-methoxy-5-(2′-ethylhexyloxy)-*p*-phenylene vinylene] (MEH-PPV). Using the variable stripe length technique in the picosecond regime, we have extensively studied the optical gain performance of asymmetric planar waveguides formed with thin MEH-PPV films spin-cast from concentrated chlorobenzene (CB) and tetrahydrofuran (THF) solutions onto thermally oxidized silicon substrates. CB and THF solvents were chosen based on their known ability to promote and effectively limit aggregate formation, respectively. Very large net gain coefficients are demonstrated, reaching values of 330 and 365 cm^{-1}, respectively, when optically pumping the waveguides with a maximum energy density of 85 $\mu J/cm^2$. Our results clearly demonstrate that polymer morphology, and hence, the chain conformation dependence of the degree of aggregation in the films as controlled by the solvent, has minimal impact on the net gain. Moreover, the waveguides exhibit low loss coefficients of 10−20 cm^{-1} at the ASE wavelength. These results question the importance of polymer morphology and aggregate formation in polymer-based optical devices operating at high excitation densities in the stimulated emission regime as would be characteristic of lasers and optical amplifiers.

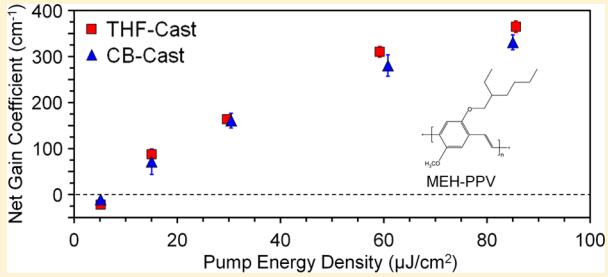

INTRODUCTION

Organic semiconductors have recently emerged as potential candidates for cost-effective optical components integrated on silicon due to encouraging success in the development of compact, solution processable, optically pumped conjugated polymer-based lasers.[1] An approach that has recently been proposed involves the incorporation of the conjugated polymer (CP) MeLPP [methyl-substituted ladder-type poly(*p*-phenylene)] into a Fabry−Perot-like cavity structure formed between two high index contrast subwavelength-sized silicon gratings.[2] Laser action has also been reported from Si-based hybrid structures involving, for example, the combination of microstructured silicon resonators with the conjugated polymer poly[2-methoxy-5-(2′-ethylhexyloxy)-*p*-phenylene vinylene] (MEH-PPV).[3] Because these organic−inorganic hybrid structures are an economical alternative to previously proposed approaches[4−7] for integration of light emission on silicon, a more comprehensive and quantitative understanding of the optical gain behavior as a function of polymer morphology is needed. Such an understanding is critical in optimizing the performance of conjugated polymer-based optical devices.

It is well accepted that the optical and electrical properties of MEH-PPV are heavily dependent on the conformational states of the polymer chains and the manner in which they are packed together in a film.[8−13] For example, in high concentration films where the polymer chains are relatively well packed, there is a strong tendency toward molecular chain aggregation, which is driven primarily by energetically favorable $\pi-\pi$ interchain interactions.[14,15] Population of these aggregate states, either by direct excitation or through transfer of energy, produces interchain species with photophysical properties significantly altered relative to that of single chain excitons. In this sense, we note that our definition of an aggregate is conceptually different than that of an agglomerate; aggregated polymer chains interact electronically, whereas agglomerated chains do not.

Studies have shown that the polymer morphology and, hence, the degree of aggregate formation in the films are highly sensitive to how the films are prepared. When a conjugated polymer like MEH-PPV is dissolved in an aromatic solvent like chlorobenzene (CB), the polymer strands adopt relatively open and well extended chain conformations, which persist into the cast film to promote chromophore aggregation through energetically favorable $\pi-\pi$ interactions. Alternatively, when dissolved in a moderately polar nonaromatic solvent like tetrahydrofuran (THF), the polymer backbone will kink and curl with the bulky side groups pointing irregularly in all

Received: May 1, 2012
Revised: September 4, 2012
Published: October 2, 2012

dx.doi.org/10.1021/jp304199u | *J. Phys. Chem. B* 2012, 116, 12835−12841

directions, which effectively limits the degree of chromophore aggregation carried over into the film.[9,10,16,17] Thus, conjugated polymer films cast from different solvents will have different degrees of interchain interactions. Differences in the degree of interchain interactions, in turn, lead to different photophysical properties including changes in exciton lifetime and quantum efficiency,[11,18] charge transport characteristics,[18] as well as the propensity of films to undergo nonlinear processes like photooxidation and exciton−exciton annihilation.[9] Changing the spin speed,[19] using different solution concentrations,[16] or altering postcast thermal[9,10,17,20] and solvent vapor[21,22] treatment conditions are also effective ways of controlling the film morphology and, hence, the organization of the polymer chains into aggregates. In this way, many of the electrical and optical properties that are critical to device performance can be controlled by varying the processing conditions.

At low pump energy before the threshold for amplified spontaneous emission, several groups have shown that a spectral characteristic of polymer aggregation is a marked change in the photoluminescence (PL) spectral line shape. For example, the PL spectra at low excitation density of thin films of MEH-PPV exhibit a diminishment of the electronic peak at 592 nm (0−0 transition) relative to the vibronic peak at 640 nm (0−1 transition) as the polymer concentration is increased.[9] The vibronic structure of the PL at low pump energy is a manifestation of the strong electron−phonon interactions involving the coupling of π-electrons to a series of stretching vibrations along the backbone of the MEH-PPV polymer chains.[23] Qualitatively similar behavior was observed for solid solutions of MEH-PPV blended in poly(9,9-dioctylfluorene) (PF)[24] as well as in poly(*para*-phenylene vinylene) (PPV)-silica nanocomposites.[25] Homogenous thin films of functionalized polythiophene[26] and poly(*para*-phenylene vinylene) (PPV)[9,17,27] derivatives also exhibit surprisingly small 0−0 peak intensities relative to the 0−1 peak intensity.[28] Optical interference and self-absorption effects were ruled out because of the sample's relatively low index dispersion[25] and optical density,[25,26,28] respectively. Several authors[25,26,29,30] have invoked the presence of two distinct emitting species to explain the anomalous evolution of the 0−0 to 0−1 peak intensity ratio with increasing active polymer concentration. The first are intrachain excitons, which exhibit solution-like spectroscopy and are favored in disordered regions of a film. The high efficiencies by which semiconducting polymers like MEH-PPV are capable of emitting light is attributed to the radiative recombination of these intrachain excitons. The second are interchain species, which are favored in highly ordered or aggregated regions. The basis of the two-emitter model is that the highest energy aggregate peak is red-shifted into approximate spectral coincidence with the 0−1 peak of the isolated exciton. Thus, an increasing aggregate concentration enhances the intensity of the 0−1 peak relative to the 0−0 peak.[28] Naturally, the two regions are coupled by efficient electronic energy transfer from high PL quantum efficiency isolated regions to low PL quantum efficiency aggregated regions,[30] which erodes the performance of conjugated polymer-based optical devices. While there have been numerous reports of optical gain from a wide variety of conjugated polymers, to our knowledge, there have been no systematic studies that quantitatively investigate the optical gain behavior as a function of polymer morphology for a fixed conjugated system, such as MEH-PPV, at pump energies ranging from below to well above the ASE threshold. In view of the favorable attributes conjugated polymers have for laser applications and the potential impact film morphology can have on device performance, such an understanding would be beneficial to the optimization of polymer-based optical devices operating at post-threshold excitation densities.

Here we report on the effect of polymer morphology and chain aggregation as altered by the chemical nature of the solvent on the ASE behavior of the conjugated polymer MEH-PPV. Using the variable stripe length technique with picosecond pulse excitation, extensive gain measurements are performed on asymmetric planar waveguides formed with thin films spin-cast from concentrated tetrahydrofuran (THF) and chlorobenzene (CB) solutions onto thermally oxidized silicon substrates. ASE threshold and waveguide loss measurements are also performed. Both CB- and THF-cast films are found to exhibit low ASE thresholds and very large optical gains. Our results conclusively show that the solvent and, hence, the chain conformation dependence of the degree of aggregate formation in the films have minimal influence on optical gain. This is advantageous because it enhances the parameter space that is accessible during device fabrication, allowing for greater flexibility in terms of optimization. In particular, the results reported here are relevant to fabrication of an electrical injection polymer laser, where some degree of chain aggregation will be required for both charge transport and stability purposes. The results reported here are also the first gain measurements on the conjugated polymer MEH-PPV that have been reported in the ps regime.

MATERIALS AND METHODS

Gilch type MEH-PPV (M_n = 286712 g/mol, M_w/M_n = 4.1, as determined by GPC) was purchased from Sigma-Aldrich and used as received. High concentration (1.0% w/v) solutions of MEH-PPV in CB (Aldrich, anhydrous, 99.8%) and distilled THF (Aldrich, anhydrous, ≥99.9%, inhibitor-free) were prepared by dissolving the appropriate amount of polymer in each solvent under a high purity nitrogen environment. To facilitate the dissolution process, the polymer solutions were sonicated for 30 min in an ultrasonic bath. After stirring the solutions for 24 h in the dark at room temperature, they were sonicated for an additional 1.5 h immediately prior to film formation. Optical quality planar waveguides were fabricated by spin-casting 120−130 nm thick films from the CB and THF solutions at 2000 rpm onto cleaned SiO_2/Si(100) substrates. The thickness of the SiO_2 is 1 μm and was thermally grown on the Si(100) substrate. The samples were then annealed under vacuum at 80 or 200 °C for 60 min to remove any residual solvent. The thickness and surface roughness of the films were measured using an atomic force microscope (Veeco Caliber) in tapping mode at a scan rate of 5 μm/s. Thickness measurements were made by scratching the polymer with a razor blade and measuring the step height at different regions of the film. As shown in Figure 1, the CB- and THF-cast films are highly uniform, exhibiting very low average surface roughness of 3.7 and 5.1 nm, respectively, with less than 4% variation in thickness per 100 μm length. To avoid any possible nonuniformity in film thickness near the edge of the substrate, the silicon substrates were cleaved before the optical measurements.

The in-plane (ordinary) refractive index of the MEH-PPV films at 640 nm, as determined by spectroscopic ellipsometry, is 1.84, which agrees with values reported in the literature.[31−34] The samples were photopumped with vertically polarized

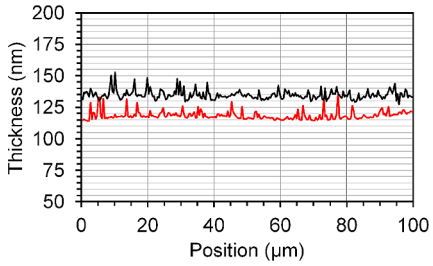

Figure 1. Film thickness variation vs position for CB- (red curve) and THF-cast (black curve) films.

pulses of 25 ps duration delivered at a repetition rate of 10 Hz using a frequency doubled (λ_{exc} = 532 nm, which is close to the absorption maximum of the polymer, namely 500 nm) regeneratively amplified mode-locked Nd:YAG (neodymium-doped yttrium aluminum garnet) laser. Pumping was performed perpendicular to the plane of the waveguides. Because the excitation pulse duration is short relative to the PL decay time of MEH-PPV, which has been reported to be ~200−300 ps,[35,36] this experiment was performed under non-steady-state conditions. Two spherical plano-convex lenses with focal lengths of 80 and 200 mm collected and collimated the emission from the edge of the films (i.e., parallel to the plane of the waveguides) and focused it onto the entrance slit of an Acton Research 2150i spectrograph coupled to a Princeton Instruments Spec-10 LN_2-cooled charge-coupled device. The collection lens was positioned at a distance of 80 mm (the focal length of the lens) from the sample edge. The energy of the pulses was controlled using a set of calibrated neutral density filters. A cylindrical lens (focal length f = 100 mm) was used to shape the pump beam into a stripe. The center portion of this stripe was then spatially filtered through a stationary metal slit to create a thin, 100 μm × 1 mm, excitation stripe on the sample surface that was oriented perpendicular to the polarization direction of the pump pulses. One end of the excitation stripe was positioned at the cleaved edge of the sample and the length of the stripe was varied by superimposing an adjustable shield directly over the fixed metal slit. The experimental arrangement used in the current work is shown in Figure 2. To minimize diffraction effects,[37] the fixed metal slit was placed in close proximity to the sample surface (~100 μm). Using the method described by Negro et al,[38] we have confirmed that the collection efficiency and excitation

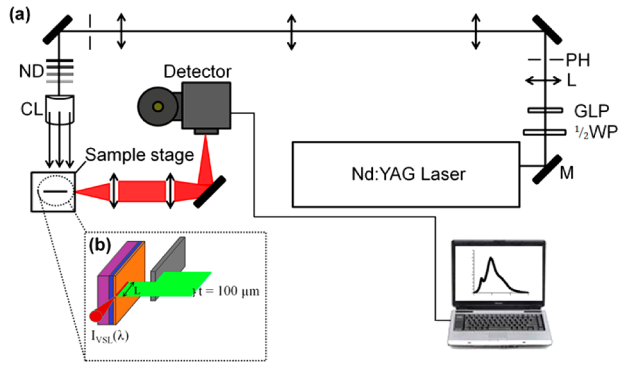

Figure 2. (a) Schematic of experimental setup: M, mirror; WP, waveplate; GLP, Glan-Laser polarizer; PH, pinhole; ND, variable neutral density filters; CL, cylindrical lens. (b) Variable stripe length (VSL) configuration.

intensity profile were effectively constant across the lengths of stripe used. All of the experiments reported here were performed under ambient conditions.

RESULTS AND DISCUSSION

In Figure 3a,b we show the edge collected photoluminescence (PL) spectra from waveguides formed with THF- and CB-cast

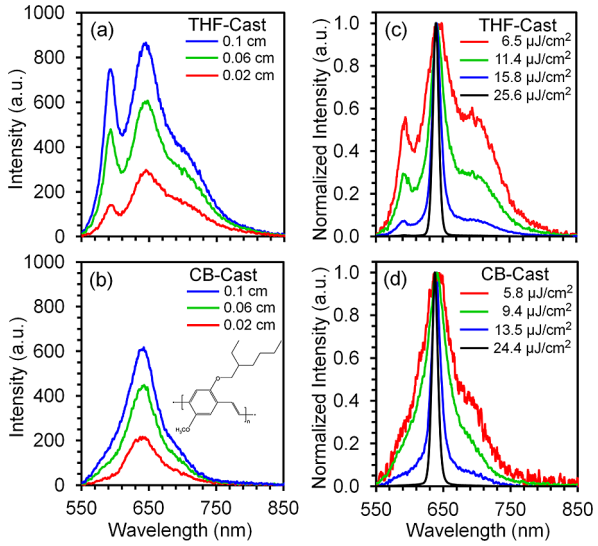

Figure 3. (a, b) PL spectra collected from the edge of waveguides formed with MEH-PPV films cast from THF and CB at different stripe lengths with a pump energy density of 5 μJ/cm^2. (c, d) Normalized spectra collected from the edge of the same waveguides at different pump energy densities with a pump stripe length of 1 mm.

films of MEH-PPV at three different stripe lengths with a low pump energy density of 5 μJ/cm^2. The PL spectra show a 0−0 transition at 592 nm followed by vibronic progressions at 640 (0−1) and 696 nm (0−2). Again, these vibronic peaks are attributed to the coupling of electronic excitations to a series of normal vibrational modes of the polymer's electronic ground state. As mentioned above, it has been postulated that the purely electronic transition at 592 nm (0−0) arises almost entirely from single chain excitons, whereas the peak intensity at 640 nm is a convolution of the highest energy aggregate emission band and the 0−1 vibronic progression associated with the single chain exciton,[25,26,29,30] which is a bimodal form of inhomogeneous broadening.[30] Thus, an increasing aggregate concentration enhances the intensity of the 0−1 peak relative to the 0−0 peak.[28] We note that when the low density PL is collected from the edge of the waveguide, self-absorption can distort the spectral line shape, predominantly at the blue edge of the PL where overlap with the absorption band is greatest.[27] In our particular case, however, self-absorption effects are minimal because there is very little overlap between the absorption and emission spectra, which is approximately the same for both the CB- and THF-cast films. That is, there is little optical density on the low energy side of the absorption band that could contribute to self-absorption. Furthermore, because the distance traveled along the waveguide is the same, any self-absorption effects would be the same and, thus, would not influence our comparison of CB- and THF-cast films. Figure 3 clearly shows that changing the solvent from THF to CB dramatically alters the PL line shape: a diminishing (0−0) 592 nm peak relative to the peak at 640 nm accompanied by a

dx.doi.org/10.1021/jp304199u | J. Phys. Chem. B 2012, 116, 12835−12841

reduction in the PL quantum yield. These emission features are consistent with prior investigations on PPV and its derivatives[9,17,28] and can be attributed to the increased degree of chain aggregation in the CB-cast films. The larger aggregate fraction in our CB-cast films is also consistent with the results of a more recent second-harmonic generation (SHG) study[39] of spin-cast films of MEH-PPV showing that the spin-speed dependence of the morphology of the polymer chains in the films is due to a competition between the rate of solvent evaporation, which kinetically traps the conformation of polymer chains in their solvent configuration, and the shear forces that are generated during spin coating, which enhances $\pi-\pi$ interaction by stretching out the polymer chains. We note that the boiling point of CB (404 K) is higher than that of THF (338 K). Thus, based on the results of the SHG study,[39] more balance between the lower evaporation rate of CB and the shear forces is expected to occur at a spin speed of 2000 rpm, which increases the degree of $\pi-\pi$ interaction in the CB-cast films. However, for both the THF- and CB-cast films, as the pump energy density is increased, the stimulated emission component increases and results in gain narrowing centered at 640 nm, which coincides with the 0−1 vibronic transition of the spontaneous emission, as shown in Figures 3c,d. Notice that the 0−1 transition shifts toward shorter wavelengths as the pump energy is increased. This blue shift coincides with the threshold for gain narrowing and indicates that ASE mainly occurs before spectral diffusion or interchain energy migration, which occurs within the first few tens of picoseconds after photoexcitation.[40−42] Thus, once population inversion is established for one of the excitonic-vibronic transitions of the low energy PL, the fast ASE process takes over and effectively shortcuts slower nonradiative recombination pathways leading to a dramatic rise in PL emission efficiency, as discussed below. We propose that such behavior is the most likely explanation for the observation of strong stimulated emission in CB-cast films, which are known to contain a large fraction of aggregates relative to films cast from THF.

In Figure 4 we show the dependence of the spectrally integrated PL intensity on the pump energy density for films annealed at 80 and 200 °C. The inset shows the corresponding variation of the PL line width. In the low pump energy regime, the integrated emission intensity for the 80 °C annealed films grows linearly with the pump energy. However, a superlinear increase in emission intensity is observed beyond a certain threshold value of the pump energy for both the THF- and CB-cast films. This abrupt rise in the PL efficiency and associated spectral narrowing are attributed to the onset of stimulated emission and is a direct indication to the presence of positive net gain. Quantitatively, we define the ASE threshold as the pump energy density at which the full width at half-maximum (fwhm) of the PL is reduced to half its low pump energy value. The deduced threshold values are, thus, 10 and 12 μJ/cm^2 for the THF- and CB-cast films annealed at 80 °C, respectively. Due to the large optical density of our MEH-PPV films at the pump wavelength, essentially all of the excitation photons incident on the films are absorbed. The spectrally integrated emission intensity is therefore proportional to the total number of emitted photons. That is, although we have not directly measured the absolute PL quantum efficiencies (QE), the relative dependence of the PL QE on casting solvent can be inferred directly from the change in slope of the integrated emission intensity at low pump energy density (Figure 4), before the threshold for ASE.[25] It has previously been shown that the threshold for ASE in a PPV derivative is correlated with the spectrally integrated low-energy PL quantum efficiency (QE).[43] We note that the low-energy PL QE of the CB-cast films is a factor of 2 lower than the THF-cast films, which is a consequence of the larger aggregate fraction in the CB-cast films. In this regard, aggregate quenching of the excited states reduces the PL efficiency of the CB-cast films by depleting the effective number of excitations that would otherwise contribute to the achievement of stimulated emission. The probability for stimulated emission is therefore reduced and the threshold shifts to larger values of pump energy, as observed in Figure 4. However, considering the relatively large drop in PL yield (factor of 2), the increase in the onset pump energy of ASE for the CB-cast films is surprisingly small, only a factor of 1.2 times larger than the THF-cast films. This small increase in the ASE threshold can be reconciled by taking into account that the waveguide loss coefficient $\alpha(\lambda)$ for the CB-cast films is nearly a factor of 2 less than the THF-cast films, as determined by shifting excitation stripe (SES) measurements shown in Figure 6. We believe that the 20% increase in the ASE threshold for the CB-cast film is mainly attributed to the reduction of the PL quantum yield that is observed at low pump energy relative to decreased loss observed in CB-cast films as discussed below. A more quantitative analysis is as follows. The threshold for amplified spontaneous emission is proportional to loss in the waveguide and inversely proportional to the quantum efficiency or the total decay time of the excited state dependent upon whether one operates in the nonsteady state[44] or steady state[31] excitation regime, respectively; for example, in our experiment of nonsteady state excitation using 25 ps pulses, $E_{th} \propto \alpha(\lambda)/\eta$, where η represents PL efficiency. All other parameters in the expression for the threshold pump energy are the same for both THF- and CB-cast films. Incorporating our values for the PL efficiencies and loss coefficients determined below into the relation above for E_{th}, we find that the ratio of threshold pump energies to be 1.21, which is entirely consistent with the 20% increase mentioned above and that the dominant factor is the difference in the PL quantum yields between the two films. It is important to point out that THF- and CB-cast films annealed at 200 °C no longer exhibit ASE threshold behavior, even when pumped at energy densities near the photodamage threshold, as shown in Figure 4. Instead, the spectrally integrated emission intensity grows linearly across *all* values of the pump energy,

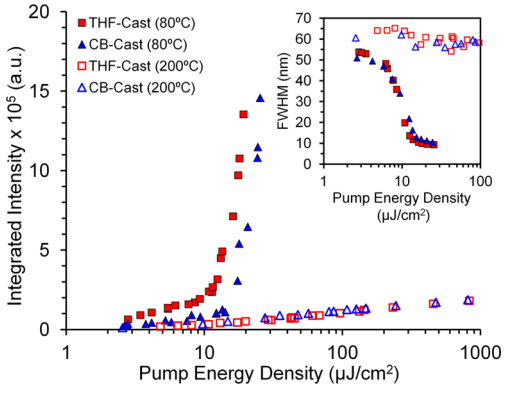

Figure 4. Dependence of the spectrally integrated, edge emitted PL intensity on pump energy density for waveguides formed with THF (squares) and CB-cast (triangles) films annealed at 80 °C (filled markers) and 200 °C (open markers). Inset shows the PL line width energy density dependence. The pump stripe length is 1 mm.

indicating that the PL efficiency has been so severely reduced that the films are no longer capable of generating a sufficiently large excitation density to support the stimulated emission; the aggregate fraction has become so large that the majority of photogenerated excited states are interchain species as opposed to isolated excitons. This is further illustrated in Figure 5, which

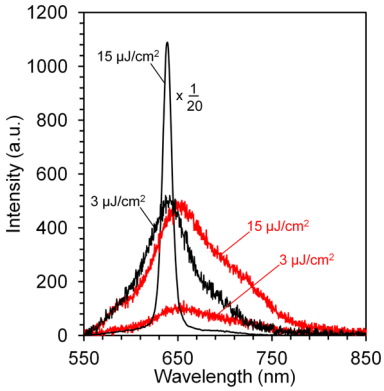

Figure 5. Emission spectra of 200 °C (red curves) and 80 °C (black curves) annealed films of MEH-PPV cast from CB at pump energy densities of 3 and 15 $\mu J/cm^2$ with a constant pump stripe length of 0.1 cm.

shows how the shape and spectral position of the PL changes when CB-cast films are annealed at 200 °C compared to 80 °C. In addition to being noticeably red-shifted, the emission spectra of the 200 °C films show considerably more emission intensity on the red side of the PL spectrum as well as dramatically lower output intensity. As noted above, these are all well-known spectral signatures attributed to an increased degree of chain aggregation in the 200 °C annealed films.[9,17,28] THF-cast films annealed at 200 °C versus 80 °C exhibit qualitatively similar behavior (curves not shown). These observations are not surprising given the extensive amount of structural relaxation that occurs at this high temperature, which is well above $T_g \sim$ 70 °C for bulk MEH-PPV used in the current work.

To characterize the effective waveguide losses we performed shifting excitation stripe (SES) measurements,[45] which involved measuring the edge emitted intensity $I_{SES}(\lambda)$ as a function of the lateral displacement x of a fixed pump stripe (1 mm × 100 μm) away from the waveguide edge. The SES data shown in

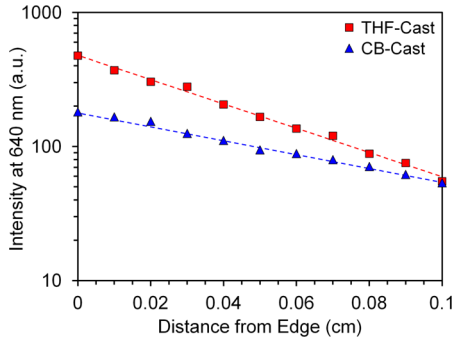

Figure 6. PL intensity at 640 nm as a function of the distance x between the sample edge and the excitation stripe for THF-cast (squares) and CB-cast (triangles) films. Data fits (broken lines) using eq 1 yields loss values of 12 and 20 cm^{-1} for CB-cast and THF-cast films, respectively.

Figure 6 were then fitted assuming an exponential dependence on the length of the unpumped region according to

$$I_{SES}(\lambda) = I_{sp}(\lambda)e^{[-\alpha(\lambda)x]} \quad (1)$$

where $\alpha(\lambda)$ is the overall loss coefficient, which includes both absorption and scattering loss, and $I_{sp}(\lambda)$ is the spontaneous emission intensity at the end of the pump stripe. Loss coefficients of 12 and 20 cm^{-1} were extracted for the waveguides formed with CB- and THF-cast films (Figure 6), respectively, which are both relatively small loss values[46] for neat, nonblended films of MEH-PPV. Neglecting other contributing factors, waveguide loss is expected to be higher in CB-cast films because of the larger fraction of aggregates. However, atomic force microscopy measurements revealed that the average surface roughness of the THF-cast films was larger than that of the CB-cast films (R_a^{THF} = 5.1 nm vs R_a^{CB} = 3.7 nm). THF-cast films were also found to exhibit a relatively large number of microvoids, which presumably formed by the rapid evaporation of solvent molecules during the spinning process. Again, we note that the boiling point of THF (338 K) is much lower than the boiling point of CB (404 K). Both the increased average surface roughness and the presence of microvoids will increase scattering loss in the THF-cast films. We suggest that it is these cumulative losses and the associated scattering of photons that most likely explain why the waveguide loss coefficient in the THF-cast films is higher than that in the CB-cast films in spite of the fact that CB-cast films exhibit a higher degree of aggregation.

The gain characteristics of the waveguides were investigated using the variable stripe length (VSL) technique.[46] To determine the net gain coefficient, $g(\lambda)$, the peak intensity, $I_{VSL}(\lambda)$, at the ASE wavelength (640 nm) was measured as a function of the pump stripe length, L, and the resulting curves were fitted to the following expression,

$$I_{VSL}(\lambda) = \frac{I_{sp}(\lambda)}{g(\lambda)}\{e^{[g(\lambda)L]} - 1\} \quad (2)$$

where $I_{sp}(\lambda)$ describes spontaneous emission, which is proportional to the pump energy. Figure 7 shows the peak intensity at λ_{ASE} for waveguides formed with THF- and CB-cast films as a function of excitation length at different pump energy

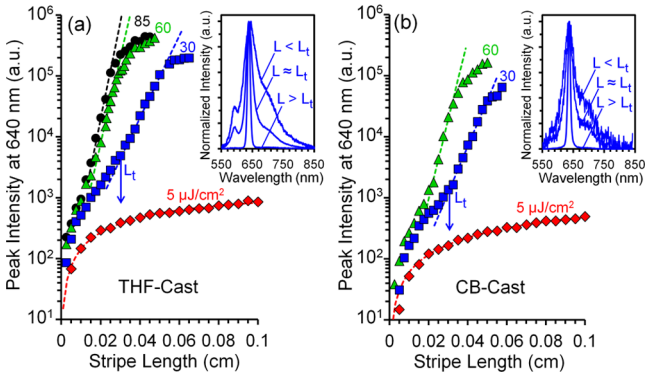

Figure 7. Excitation length dependence of the peak intensity at λ_{ASE} for waveguides formed with THF- (a) and CB-cast (b) films at different pump energy densities. The fitting to eq 2 is given by the dashed lines. The inset shows the normalized PL spectra collected at three different stripe lengths with a pump energy density of 30 $\mu J/cm^2$. The threshold excitation length L_t is indicated.

dx.doi.org/10.1021/jp304199u | J. Phys. Chem. B 2012, 116, 12835−12841

densities. It is clearly observed that at a pump energy density of 30 μJ/cm^2 an exponential increase in the peak intensity at λ_{ASE} accompanied by spectral narrowing occurs above a threshold excitation length L_t (see inset in Figure 7), which decreases as the pump energy density is increased. This decrease in L_t is a consequence of the higher gain. Note that the ASE peak intensity deviates from the exponential increase at longer excitation lengths due to gain saturation. Across this saturation stripe length regime the high level of optical amplification depletes a substantial fraction of the population inversion, leading to a reduction in the net gain.[46] Thus, in determining the net gain coefficient we used only the exponential subset of the data. It should be noted that this saturation behavior is not attributed to photodegradation of the films as subsequent scans on the same region of the film for each value of the pump energy yielded no significant changes in ASE intensity at a particular value of the excitation stripe length. In Figure 8, we

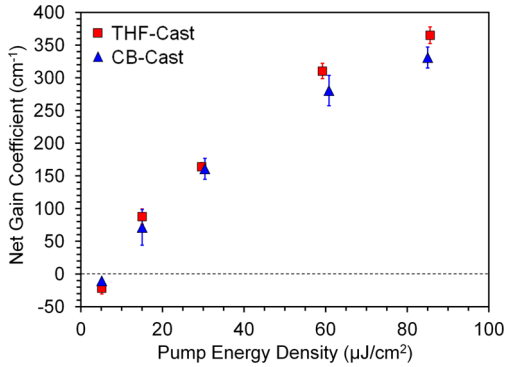

Figure 8. Net gain coefficient as a function of pump energy density for waveguides formed with THF- (squares) and CB-cast (triangles) films. Error bars indicate 2× the standard error.

show the net gain coefficient as a function of pump energy density for the CB- and THF-cast films. At a low pump energy density of 5 μJ/cm^2, the net gain coefficient for the THF- and CB-cast films are −21 and −10 cm^{-1}, respectively, indicating a loss. These loss values are in good agreement with the loss values obtained using the SES technique (Figure 6), which confirms that our experimental setup for VSL measurements[38] is configured properly. As the pump energy density is increased, both the THF- and CB-cast films exhibit very large positive net gain, reaching values of 365 and 330 cm^{-1}, respectively, when pumped at a maximum energy density of 85 μJ/cm^2. Contrary to the common perception that chain aggregation is detrimental to the ASE behavior,[17] these data clearly demonstrate that the increased aggregation in CB-cast films has little effect on optical gain; in fact, *very large* net gain can still be achieved in spite of the relatively larger aggregate concentration. These results are consistent within the framework of radiative lifetime shortening upon achieving ASE,[47−49] which leaves significantly less time for energy migration to low energy aggregate sites and subsequent quenching of the excited states. However, as the 200 °C data in Figure 4 show, polymer morphology can become significantly influential over the optical properties under conditions where extremely large aggregate fractions are formed, that is, stimulated emission is suppressed at elevated temperatures *significantly* above T_g.

It is important to note that the gain coefficients found in the current work are 4−5 times larger than what has previously been reported for MEH-PPV[31,46,50,51] and other PPV-based derivatives,[51] and, to the best of our knowledge, are the largest values reported to date for thin conjugated polymer films.[47,50−53] We have found, however, that these same waveguide structures exhibit markedly lower net gain under quasi steady-state excitation conditions using nanosecond pump pulses. A net gain of 75 cm^{-1} was achieved for 8−10 ns pump pulses at a maximum pump energy density of 1.8 mJ/cm^2 (corresponding to a pump intensity of 200 kW/cm^2), which is in good agreement with previously reported values for MEH-PPV[31,51] and related PPV derivatives[46,51] under 6−10 ns pulse conditions. The lower net gain obtained under quasi-steady-state excitation conditions is currently believed to be due to localized photochemical and photothermal changes in film morphology induced by the relatively long duration, high energy ns pump pulses.[9,48] No photodamage to the samples was observed under picosecond pulsed excitation. Compared to THF-cast films, the relatively higher aggregate concentration in the CB-cast films affects only slightly (<15%) the net gain for both ps and ns pulses. That is, the solvent dependence of the degree of aggregation in the films and its influence on the ASE behavior of MEH-PPV is preserved in both excitation regimes. The pulse width dependence, that is, non-steady-state versus quasi-steady-state excitation, of the ASE behavior is beyond the scope of the current work and will be the subject of a subsequent publication.

CONCLUSIONS

In summary, we have presented the results of a detailed study investigating the morphology dependence of optical gain in thin spin-cast films of MEH-PPV. The polymer morphology and extent of aggregate formation in the films was controlled by altering the chemical nature of the solvent from which the films were cast. Chlorobenzene (CB) and tetrahydrofuran (THF) were chosen based on their known ability to promote and effectively limit aggregate formation, respectively. Although films cast from CB were found to exhibit a significantly lower PL efficiency at low pump energy compared to films cast from THF, our variable stripe length measurements in the ps regime showed little difference (<15%) in optical gain above the ASE threshold. Both the CB- and THF-cast films exhibited very large gain coefficients, reaching values of 330 and 365 cm^{-1}, respectively, at a maximum pump energy density of 85 μJ/cm^2. Loss measurements revealed low loss coefficients of 10−20 cm^{-1}. These results clearly demonstrate that the film morphology and aggregation state of the polymer chains as controlled by the chemical nature of the solvent has minimal influence on the optical gain properties of thin spin-cast films of MEH-PPV. Our data therefore suggest that the impact of polymer morphology on device performance depends upon the operational regime, spontaneous versus stimulated emission, of the actual device. Furthermore, the present results make evident the fact that very large net gains and low losses can still be achieved from MEH-PPV films without the need for complex processing techniques involving, for example, the encapsulation of polymer chains in the nanopores of a silica host, as has recently been proposed.[50] The results reported here may have important implications for the construction and optimization of an electrically pumped laser device where some degree of aggregation will be required for charge transport purposes.

AUTHOR INFORMATION

Corresponding Author

*E-mail: zelamper@ncsu.edu.

Notes

The authors declare no competing financial interest.

REFERENCES

(1) Turnbull, G. A.; Andrew, P.; Barnes, W. L.; Samuel, I. D. W. *Appl. Phys. Lett.* **2003**, *82*, 313−315.
(2) Stoferle, T.; Moll, N.; Wahlbrink, T.; Bolten, J.; Mollenhauer, T.; Scherf, U.; Mahrt, R. F. *Nano Lett.* **2010**, *10*, 3675−3678.
(3) Vasdekis, A. E.; Moore, S. A.; Ruseckas, A.; Krauss, T. F.; Samuel, I. D. W.; Turnbull, G. A. *Appl. Phys. Lett.* **2007**, *91*, 0511241−0511243.
(4) Cloutier, S. G.; Kossyrev, P. A.; Xu, J. *Nat. Mater.* **2005**, *4*, 887−891.
(5) Fang, A. W.; Park, H.; Cohen, O.; Jones, R.; Paniccia, M. J.; Bowers, J. E. *Opt. Express* **2006**, *14*, 9203−9210.
(6) Makarova, M.; Vuckovic, J.; Sanda, H.; Nishi, Y. *Appl. Phys. Lett.* **2006**, *89*, 3.
(7) Pavesi, L.; Dal Negro, L.; Mazzoleni, C.; Franzo, G.; Priolo, F. *Nature* **2000**, *408*, 440−444.
(8) Nguyen, T. Q.; Kwong, R. C.; Thompson, M. E.; Schwartz, B. J. *Appl. Phys. Lett.* **2000**, *76*, 2454−2456.
(9) Nguyen, T. Q.; Martini, I. B.; Liu, J.; Schwartz, B. J. *J. Phys. Chem. B* **2000**, *104*, 237−255.
(10) Nguyen, T. Q.; Schwartz, B. J.; Schaller, R. D.; Johnson, J. C.; Lee, L. F.; Haber, L. H.; Saykally, R. J. *J. Phys. Chem. B* **2001**, *105*, 5153−5160.
(11) Collison, C. J.; Rothberg, L. J.; Treemaneekarn, V.; Li, Y. *Macromolecules* **2001**, *34*, 2346−2352.
(12) Zheng, M.; Bai, G. L.; Zhu, D. B. *J. Photochem. Photobiol., A* **1998**, *116*, 143−145.
(13) Hu, D. H.; Yu, J.; Wong, K.; Bagchi, B.; Rossky, P. J.; Barbara, P. F. *Nature* **2000**, *405*, 1030−1033.
(14) Chen, S. H.; Su, A. C.; Chou, H. L.; Peng, K. Y.; Chen, S. A. *Macromolecules* **2003**, *37*, 167−173.
(15) Yang, C. Y.; Hide, F.; Díaz-García, M. A.; Heeger, A. J.; Cao, Y. *Polymer* **1998**, *39*, 2299−2304.
(16) Nguyen, T. Q.; Doan, V.; Schwartz, B. J. *J. Chem. Phys.* **1999**, *110*, 4068−4078.
(17) Schwartz, B. J. *Annu. Rev. Phys. Chem.* **2003**, *54*, 141−172.
(18) Lee, T. W.; Park, O. O. *Adv. Mater.* **2000**, *12*, 801−804.
(19) Shi, Y.; Liu, J.; Yang, Y. *J. Appl. Phys.* **2000**, *87*, 4254−4263.
(20) Samuel, I. D. W.; Turnbull, G. A. *Chem. Rev.* **2007**, *107*, 1272−1295.
(21) Li, G.; Yao, Y.; Yang, H.; Shrotriya, V.; Yang, G.; Yang, Y. *Adv. Funct. Mater.* **2007**, *17*, 1636−1644.
(22) Vogelsang, J.; Brazard, J.; Adachi, T.; Bolinger, J. C.; Barbara, P. F. *Angew. Chem., Int. Ed.* **2011**, *50*, 2257−2261.
(23) Hagler, T. W.; Pakbaz, K.; Voss, K. F.; Heeger, A. J. *Phys. Rev. B* **1991**, *44*, 8652−8666.
(24) Liu, J.; Shi, Y. J.; Yang, Y. *Appl. Phys. Lett.* **2001**, *79*, 578−580.
(25) Ho, P. K. H.; Kim, J. S.; Tessler, N.; Friend, R. H. *J. Chem. Phys.* **2001**, *115*, 2709−2720.
(26) Brown, P. J.; Thomas, D. S.; Kohler, A.; Wilson, J. S.; Kim, J. S.; Ramsdale, C. M.; Sirringhaus, H.; Friend, R. H. *Phys. Rev. B* **2003**, *67*, 064203.
(27) Meskers, S. C. J.; Janssen, R. A. J.; Haverkort, J. E. M.; Wolter, J. H. *Chem. Phys.* **2000**, *260*, 415−439.
(28) Spano, F. C. *J. Chem. Phys.* **2005**, *122*, 15.
(29) Bjorklund, T. G.; Lim, S. H.; Bardeen, C. J. *Synth. Met.* **2004**, *142*, 195−200.
(30) Wang, P.; Cuppoletti, C. M.; Rothberg, L. J. *Synth. Met.* **2003**, *137*, 1461−1463.
(31) Lahoz, F.; Oton, C. J.; Capuj, N.; Ferrer-Gonzalez, M.; Cheylan, S.; Navarro-Urrios, D. *Opt. Express* **2009**, *17*, 16766−16775.
(32) Bahtiar, A.; Koynov, K.; Ahn, T.; Bubeck, C. *J. Phys. Chem. B* **2008**, *112*, 3605−3610.
(33) Koynov, K.; Bahtiar, A.; Ahn, T.; Bubeck, C.; Horhold, H. H. *Appl. Phys. Lett.* **2004**, *84*, 3792−3794.
(34) Koynov, K.; Bahtiar, A.; Ahn, T.; Cordeiro, R. M.; Horhold, H. H.; Bubeck, C. *Macromolecules* **2006**, *39*, 8692−8698.
(35) Hu, D. H.; Yu, J.; Barbara, P. F. *J. Am. Chem. Soc.* **1999**, *121*, 6936−6937.
(36) Smilowitz, L.; Hays, A.; Heeger, A. J.; Wang, G.; Bowers, J. E. *J. Chem. Phys.* **1993**, *98*, 6504−6509.
(37) Khriachtchev, L.; Rasanen, M.; Novikov, S.; Sinkkonen, J. *Appl. Phys. Lett.* **2001**, *79*, 1249−1251.
(38) Dal Negro, L.; Bettotti, P.; Cazzanelli, M.; Pacifici, D.; Pavesi, L. *Opt. Commun.* **2004**, *229*, 337−348.
(39) Craig, I. M.; Tassone, C. J.; Tolbert, S. H.; Schwartz, B. J. *J. Chem. Phys.* **2010**, *133*, 11.
(40) Wegmann, G.; Schweitzer, B.; Hertel, D.; Giessen, H.; Oestreich, M.; Scherf, U.; Mullen, K.; Mahrt, R. F. *Chem. Phys. Lett.* **1999**, *312*, 376−384.
(41) Hide, F.; Schwartz, B. J.; Díaz-García, M. A.; Heeger, A. J. *Chem. Phys. Lett.* **1996**, *256*, 424−430.
(42) Hayes, G. R.; Samuel, I. D. W.; Phillips, R. T. *Phys. Rev. B* **1995**, *52*, R11569−R11572.
(43) Spiegelberg, C.; Peyghambarian, N.; Kippelen, B. *Appl. Phys. Lett.* **1999**, *75*, 748−750.
(44) Wang, S. M.; Liu, X. Y.; Wang, L. J.; Li, W. L.; Lee, S. T. *Thin Solid Films* **2000**, *363*, 182−184.
(45) Valenta, J.; Pelant, I.; Linnros, J. *Appl. Phys. Lett.* **2002**, *81*, 1396−1398.
(46) McGehee, M. D.; Gupta, R.; Veenstra, S.; Miller, E. K.; Diaz-Garcia, M. A.; Heeger, A. J. *Phys. Rev. B* **1998**, *58*, 7035−7039.
(47) Frolov, S. V.; Vardeny, Z. V.; Yoshino, K. *Phys. Rev. B* **1998**, *57*, 9141−9147.
(48) Frolov, S. V.; Shkunov, M.; Fujii, A.; Yoshino, K.; Vardeny, Z. V. *IEEE J. Quantum Electron.* **2000**, *36*, 2−11.
(49) Frolov, S. V.; Gellermann, W.; Ozaki, M.; Yoshino, K.; Vardeny, Z. V. *Phys. Rev. Lett.* **1997**, *78*, 729−732.
(50) Martini, I. B.; Craig, I. M.; Molenkamp, W. C.; Miyata, H.; Tolbert, S. H.; Schwartz, B. J. *Nat. Nanotechnol.* **2007**, *2*, 647−652.
(51) de la Rosa-Fox, N. *Opt. Mater.* **1999**, *12*, 267−271.
(52) Heliotis, G.; Bradley, D. D. C.; Turnbull, G. A.; Samuel, I. D. W. *Appl. Phys. Lett.* **2002**, *81*, 415−417.
(53) Song, M. H.; Wenger, B.; Friend, R. H. *J. Appl. Phys.* **2008**, *104*, 033107.